

RESEARCH

Open Access



Electroacupuncture attenuates intervertebral disc degeneration by upregulating aquaporins via the cAMP/PKA pathway

Min Wang^{1†}, Jia-Bao Huang^{2†}, Jing Zou³ and Guo-fu Huang^{1,4*}

Abstract

Background Intervertebral disc degeneration (IVDD) is characterized by a decrease in extracellular matrix (ECM) and water loss, which is a major cause of low back pain (LBP). Electroacupuncture (EA) has long been used to relieve LBP in IVDD. To investigate whether EA can upregulate aquaporins (AQPs) in IVDD via the cAMP/PKA pathway in a rabbit model of disc degeneration.

Methods A homemade loading device was adapted to trigger a disc degeneration model. After 28 days, EA treatment was performed. Magnetic resonance imaging (MRI), diffusion-weighted imaging (DWI), and diffusion tensor imaging (DTI) were performed to evaluate AQP content and water diffusion. AQP protein expression in the slices was observed by Western blot and immunofluorescence (IF) staining. The pathology of the intervertebral discs was determined by staining. cAMP and PKA levels were examined using ELISA, and the expression of AQP genes as well as the cAMP/PKA pathway and its related molecules were examined using quantitative reverse transcription-PCR (qRT-PCR) and Western blot analysis.

Results The EA intervention reduced MRI Pfirrmann scores, fractional anisotropy (FA), and apparent diffusion coefficient (ADC) values. EA can upregulate the expression of AQP1 and AQP3, thereby improving the pathological morphology of the nucleus pulposus (NP) and the cartilage endplate of the intervertebral disc. cAMP and PKA levels were significantly increased after EA intervention in rabbits with IVDD. EA intervention can partially improve the expression of related molecules in the cAMP/PKA pathway, but H-89 reverses the effect of EA.

Conclusion EA can attenuate intervertebral disc degeneration by regulating AQP expression, a process that may be mediated by the cAMP/PKA pathway.

Keywords Electroacupuncture, Intervertebral disc degeneration, Aquaporin 1, Aquaporin 3, cAMP/PKA pathway

[†]Min Wang and Jia-Bao Huang contributed equally to this work and share first authorship.

*Correspondence:

Guo-fu Huang
531529128@qq.com

¹School of Acupuncture and Bone, Hubei University of Chinese Medicine, No. 1 Huangjiahu West Road, Hongshan District, Wuhan, Hubei 430065, China

²Department of Rehabilitation Medicine, The First Affiliated Hospital, Sun Yat-sen University, Guangzhou, Guangdong, China

³Department of Acupuncture & Moxibustion, Wuhan No.1 Hospital, Wuhan, Medicine Tongji Medical College of Huazhong University of Science and Technology, Wuhan Hospital of Integrated Chinese & Western Medicine, NO. 215 Zhongshan Road, Wuhan, Hubei 430022, China

⁴Longgang District Maternity & Child Healthcare Hospital of Shenzhen City (Longgang Maternity and Child Institute of Shantou University Medical College), NO.6 Ailong Road, Longcheng Street, Central City, Longgang District, Shenzhen City, Guangdong 518172, China



Introduction

Intervertebral disc degeneration (IVDD) is the most common cause of functional impairment and pain in the lower back and represents a significant social and economic burden for approximately 80% of the world's population [1, 2]. Previous studies have shown that the underlying cause of IVDD is tissue degeneration, which can be influenced by various factors such as: Impairment of metabolite transport, cell aging and death, genetic inheritance, changes in matrix macromolecules and water content, changes in enzyme activity and structural failure and neurovascular ingrowth [3–7]. Although studies have shown that IVDD involves a cascade of cellular, biochemical, and structural changes, the initiating events leading to IVDD are not well understood. Two features that uniquely characterize the intervertebral disc are hypoxia [8, 9] and increased osmolarity, which results in high water content in the tissue [10]. The water content of the intervertebral disc nucleus exceeds 80% in childhood, decreasing to approximately 70% in older age. As we age, the intervertebral discs are very susceptible to degeneration caused by loss of swelling pressure and fluid supply [11, 12]. Therefore, water content is an important factor underlying the mechanisms of lumbar intervertebral disc degeneration. Dehydration of the intervertebral disc, as seen in IVDD, contributes to the pathogenesis of degenerative disc disease [13].

Aquaporins (AQPs), a class of transmembrane proteins, function primarily to transport water molecules across the membrane and are thought to play a role in the natural history of intervertebral disc degeneration [14]. The expression of AQP1 and AQP3 has been demonstrated in the intervertebral disc [15]. Since the intervertebral disc is a vascular tissue, the endplate pathway was found to be the main route of nutrition and water transport in the intervertebral disc [16]. The transport of AQP1, 3 is closely related to cartilage endplate hydration and intervertebral disc degeneration. Blocking this pathway leads to a significant reduction in diffusive transport to the nucleus pulposus and subsequent loss of the extracellular matrix (ECM). The decreased expression of AQPs from the disc nucleus to the annulus fibrosus reflects differences in mechanobiology, permeability, and hydration between these regions [17, 18].

Electroacupuncture (EA) is a therapy based on traditional acupuncture combined with modern electrotherapy. EA has been shown to significantly promote the recovery of neurological functions, relieve neuropathic pain and thus improve quality of life [19, 20]. In addition, EA has long been used to treat back pain [21]. It has been found in many clinical studies to be effective in relieving back pain by producing an analgesic effect, lowering the pain threshold, improving physical activity and sleep quality, and reducing the daily need for oral analgesics

[22]. Our previous study [23, 24] found that EA had anabolic and anticatabolic effects on the regulation of extracellular matrix in intervertebral discs. EA increased ECM content and showed evidence of regenerative potential in degenerated discs assessed by protein expression and magnetic resonance imaging. Furthermore, EA suppresses neuropathic pain caused by spinal nerve ligation by improving neuronal plasticity through upregulation of the cAMP/PKA signaling pathway [25].

In the current study, we hypothesize that EA can mitigate intervertebral disc degeneration by upregulating the expression of AQPs via the cAMP/PKA pathway. We investigated the involvement of AQPs in the effect of EA on IVD degeneration and the relationship between AQP content, IVDD, and the levels of the cAMP/PKA signaling pathway and its associated molecules in the lumbar disc.

Materials and methods

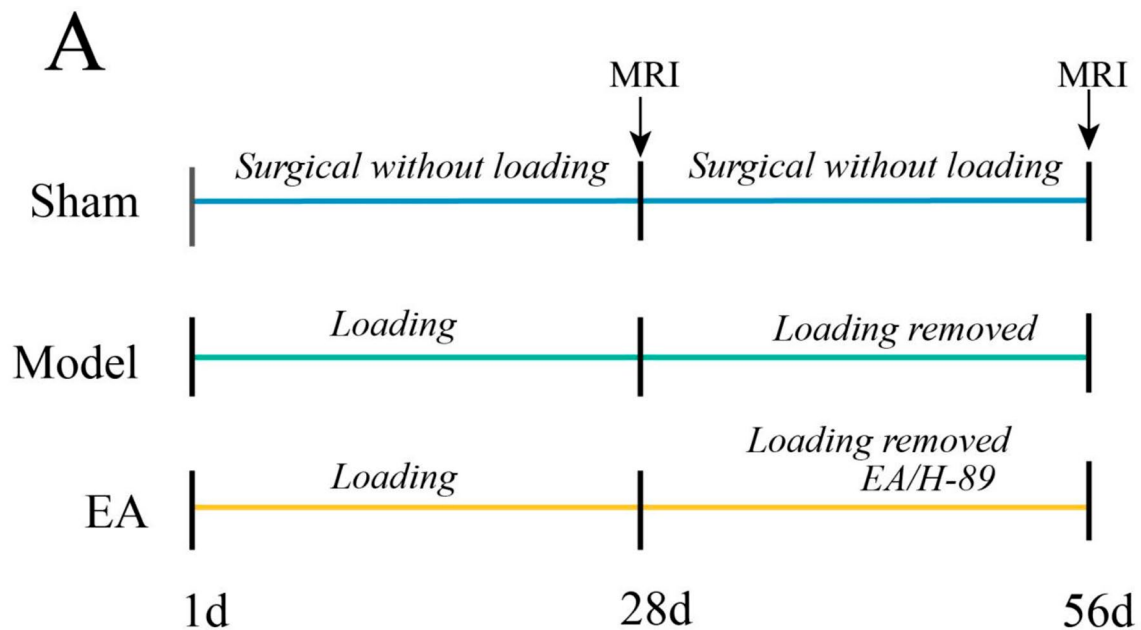
Animals and experimental protocol

Experiments were conducted using male adult New Zealand rabbits weighing 3–4 kg. All procedures were approved by the Animal Care Committee of Wuhan Hospital of Integrated Chinese & Western Medicine. A total of 27 experimental animals were used, with 8 randomly selected as the sham-operated group. The remaining animals underwent the induction of IVDD models. Different interventions were carried out on the 1st, 28th, and 56th days [26, 27] (Figure.1 A). The IVDD model was established in accordance with the protocol described by Kroeber MW [28]. Rabbits were anesthetized using pentobarbital sodium (30 mg/kg) administered via the marginal ear vein. A dorsal approach to the lumbar spine was used to attach a custom-made loading device to two Kirschner wires (1.5 mm in diameter). These wires were inserted into the L4 and L5 vertebral bodies parallel to the adjacent study slice using a variable-speed electric drill. After the wound was sutured, axial compression was applied to the disc using a spring within the device, generating a compression force of 200 N to induce disc degeneration [29] (Figure.1B). The sham group underwent the same procedure, but the external compression device was positioned without applying any compressive force. The rabbits received intramuscular injections of penicillin sodium (4×10^6 U) once daily for 5 days postoperatively. The modeling device was removed on the 28th day, after which the intervertebral discs were scanned using MRI. The EA group received EA treatment starting from the first day after successful modeling, and some animals also received an injection of the H-89 inhibitor.

Magnetic resonance imaging

On day 28, magnetic resonance imaging (MRI) was performed for each group. Imaging was performed 30 min after the removal of the external fixator. Imaging was performed using a 3.0T MRI scanner (GE Healthcare, American) with spin-echo echo-planar imaging (SE-EPI) acquisition in the sagittal view with the following scanning parameters: repetition time/time echo (TR/TE)=2300 ms/64.9 ms, slice thickness/spacing (thn/spa)=4 mm/1 mm, acquisition matrix=128×64, field of view (FOV)=34 cm, number of excitations (NEX)=4. Sagittal diffusion tensor imaging scanning was performed with SE-EPI under the following parameters [30]: TR/TE=2500 ms/80.8, thn/spa=4 mm/1 mm, matrix=128×64, FOV=34 cm, NEX=4, B-value=800, diffusion direction=13 and scan time of one minute and 15 s. T2* mapping was acquired by gradient recall echo

(GRE) as follows. The acquired T2-weighted (T2W) images were examined by two radiologists, each with more than ten years of experience, to assess the degree of disc degeneration. For the assessment of intervertebral disc degeneration, the Pfirrmann classification was used, ranging from grades 1 (normal) to 5 (severe degeneration with transition to herniation). The raw diffusion-weighted imaging (DWI) and diffusion tensor imaging (DTI) data were transferred to the Workstation 4.2 and processed using GE Healthcare's Functool software to produce apparent diffusion coefficient (ADC), fractional anisotropy (FA), and pseudocolor images. On the intermediate layer of the ADC sagittal image, the central regions of the nucleus pulposus (NPs) were marked as regions of interest (ROIs) to measure the ADC values. Furthermore, fractional anisotropy (FA) values were measured using the same method as described above.



B

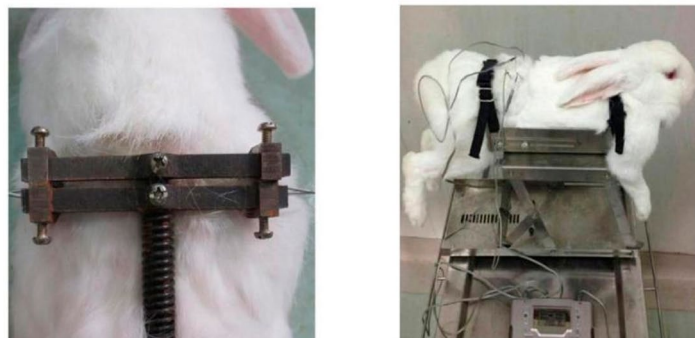


Fig. 1 Diagram and model of the experimental protocol. This figure illustrates the surgical procedure used for inducing IVDD in New Zealand rabbits, including the placement of the custom-made loading device and the application of axial compression. The sham-operated group is also depicted, showing the procedure without the application of compressive force

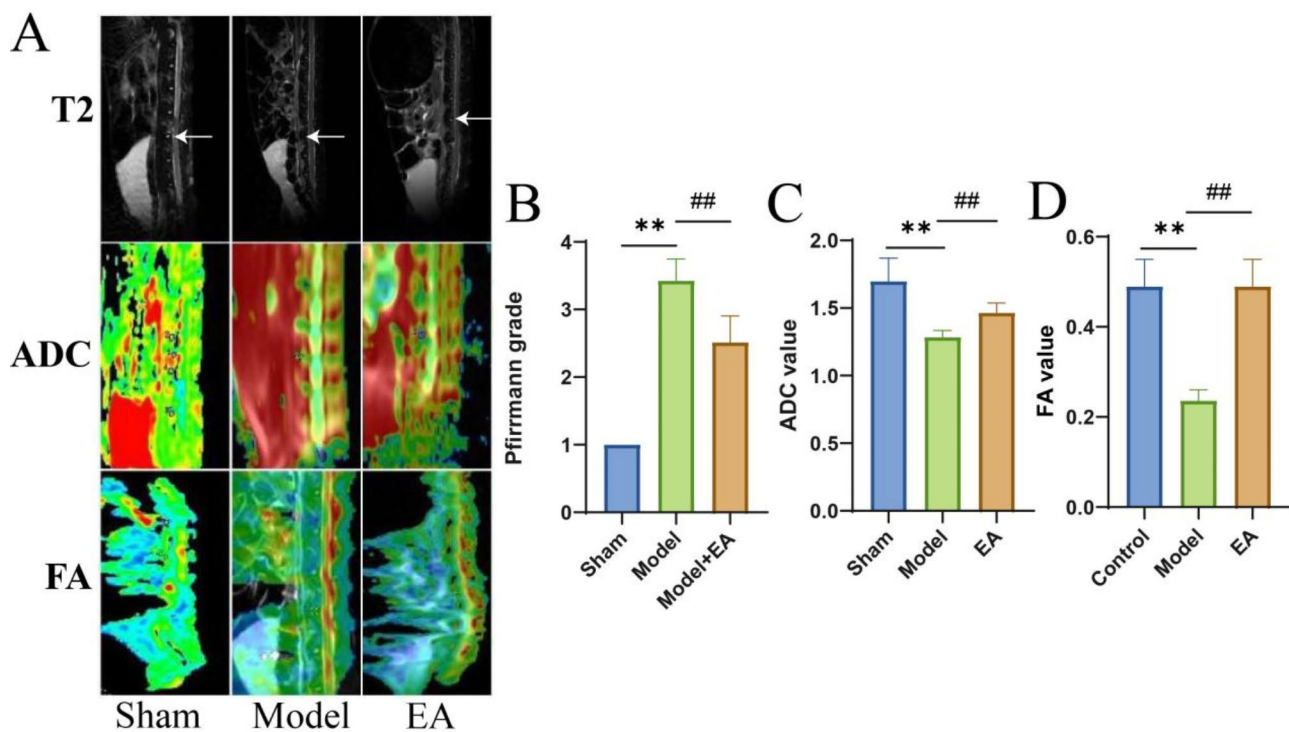


Fig. 2 MRI images of the lumbar spine. (A) T2-weighted images, apparent diffusion coefficient (ADC) pseudocolor images, and fractional anisotropy (FA) pseudocolor images are listed from top to bottom, respectively. (B) The bar graph shows the Pfirrmann classification at 56 days. (C–D) The bar graphs show the ADC and FA values at 56 days. Data are expressed as mean \pm SD. ** $P < 0.01$ indicates significant differences compared to the sham compressed group, and ## $P < 0.01$ compared to the model group

EA treatment

A multifunctional solid support was used for the EA treatment (Fig. 2.B). The procedure was as follows: the rabbits were fixed on the operating table, and the Jiaji” (EX-B2) points on both sides of the L4 and L5 vertebrae were located according to the literature [31]. 0.30 mm \times 25 mm acupuncture needles were inserted perpendicularly to a depth of 0.5–0.8 cm. The Han’s acupoint nerve stimulator (Beijing, China) was then connected. The intensity of the acupoint nerve stimulator was 1 mA, and the frequency was 2 Hz/15 Hz. EA was performed once daily, with each session lasting 20 min. Each treatment course consisted of 6 consecutive days, with a 1-day interval between courses, totaling 4 courses [32, 33].

Tissue preparation

After the experiment, the animals were humanely euthanized via rapid air injection into the marginal vein of the ear. The complete intervertebral discs were then removed and divided into two symmetrical parts. One portion was immediately snap-frozen in liquid nitrogen for subsequent Enzyme-Linked Immunosorbent Assay (ELISA), Western blot, and quantitative reverse transcription-PCR (qRT-PCR) analyses, while the second part was used for hematoxylin and eosin (HE) staining, toluidine blue O (TBO) staining, and immunofluorescence.

Table 1 Antibody Dilution ratio

Antibody	Catalog Number	Dilution Ratio	Source
mouse anti-AQP1	NB600-749	1:200	Novus, USA
rabbit anti-AQP3	ab125219	1:200	abcam, UK
Goat Anti-Mouse IgG	SAB51375	1:300	Bioswamp, China
Goat Anti-Rabbit IgG	SAB51371	1:300	Bioswamp, China

Immunofluorescence

Formalin-fixed disc samples were embedded in paraffin and cut into 5- μ m-thick sections. IF staining was then performed according to the manufacturer’s protocols. The antibodies used for IF staining are listed in Table 1. All brightfield images were captured using a microscope (EVOS flauto, Thermo Fisher Scientific, USA) and analyzed with Image-Pro Plus 6.0 (USA).

HE staining

The intervertebral disc tissue fixed in paraformaldehyde was retrieved and then underwent routine dehydration and paraffin embedding, thus being made into paraffin sections with a thickness of 5 μ m. The process encompassed several steps: section picking, followed by baking, rinsing, and dewaxing; then hematoxylin staining, dehydration, and transparency; subsequently, sealing with

neutral resin. Finally, the sections were observed under an optical microscope, and images were captured for subsequent analysis.

TBO staining

The intervertebral disc tissue was dewaxed until it was hydrated. Toluidine blue staining solution was added dropwise, and the tissue was stained for 20 to 30 min. Then, the excess staining solution was washed away. Color separation was performed using 95% ethanol, and the color separation effect was controlled under the microscope. For dehydration and transparency, the tissue was immersed in absolute ethanol for 1 min, followed by immersion in xylene three times for 1–2 min each, and finally sealed with neutral gum. Staining results: Chondrocytes and osteoblasts appeared bluish-purple, while the background was light blue.

ELISA assay

The cAMP and PKA levels in the disc were quantified using ELISA kits from Gene Beauty Biotechnology Co., Ltd.(Wuhan, China). The test was performed according to the manufacturer's instructions. The plates were read on the Labsystems Multiskan MS plate reader (Vantaa, Finland) at a wavelength of 450 nm. The values thus obtained were plotted on a standard chart prepared using serial dilutions of the standard provided with the kit, and the cAMP and PKA concentrations were calculated.

qRT-PCR

Total RNA was isolated using the Trizol reagent kit (Ambion, Austin, TX, USA) and converted to complementary DNA (cDNA) using the Revert Tra Ace First Strand cDNA Synthesis Kit (Kapa Biosystems, Boston, MA, USA). Real-time PCR was performed using the Premix Ex Taq kit (Takara, Japan) and a BIO-RAD CFX96 real-time PCR system (BIO-RAD, Hercules, CA, USA) according to the manufacturer's instructions. The mRNA expression levels of AQP1, AQP3, p-CREB, eIF-2, actin, MAP1A, MAP1B, MAP2, MAP4, and tau were normalized to the endogenous expression of GAPDH. The primers were sourced from Nanjing Kingsy Biotechnology Co., Ltd. (Nanjing, China). The relative copy number of the target genes, normalized to GAPDH, was determined using the $2^{-\Delta\Delta Ct}$ method [34]. The primer pairs selected for qRT-PCR are listed in Table 2.

Western blot analysis

The disc tissue was quickly removed and homogenized in ice-cold lysis buffer (50 mM Tris-HCl, pH 7.5). Total protein was extracted from the tissue using RIPA lysis buffer with a tissue homogenizer and then centrifuged at 4 °C for 10 min at 15,000 g to obtain the total protein extract in the supernatant. Protein concentrations were

Table 2 Sequences of primers

Primers	sequences	Length (bp)
AQP1-F	5'- TGCTCATCTACGACTTT – 3'	139
AQP1-R	5'- TATTTGGGTTTCATCTC – 3'	
AQP3-F	5'- CGTGAAGCACAAAGGAGCA – 3'	138
AQP3-R	5'- GTGAGGGGACAGAGGGCAG – 3'	
CREB-F	5'- ACGACAAATCATCTCTC – 3'	131
CREB-R	5'- TGTTCTGAATCCACTA – 3'	
eIF2-F	5'- CTACTTTGTGCCGTGCT – 3'	149
eIF2-R	5'- TTTCGCTGCTTTCTTGT – 3'	
ACTIN-F	5'- GATCTGGCCTACTCC – 3'	114
ACTIN-R	5'- ATCTCGCACGCTTTCT – 3'	
MAP1A-F	5'- TCGTGCGAGTGCTTTTT – 3'	113
MAP1A-R	5'- CAGGTCCTTCTGGGTGG – 3'	
MAP1B-F	5'- GTCCTGTCCCTTTTGA – 3'	187
MAP1B-R	5'- GGTGGCGGATGAGTTTC – 3'	
MAP2-F	5'- GAAGACAGAACCAAGCC – 3'	131
MAP2-R	5'- GAGCAACTAAACCCAC – 3'	
MAP4-F	5'- ATCAGAACAGCCAGAACT – 3'	134
MAP4-R	5'- ACTAGAGAGAAACAGCAA – 3'	
TAU-F	5'- GGATGAGGACCAGGACA – 3'	151
TAU-R	5'- GGCAACTTTGGAGAGGA – 3'	
GAPDH-F	5'- ACCCACTCCTCTACCTTCG – 3'	108

Table 3 Antibody Dilution ratio

Antibody	Catalog Number	Dilution Ratio	Source
mouse anti-AQP1	NB600-749	1:1000	Novus, USA
rabbit anti-AQP3	ab125219	1:1000	abcam, UK
Mouse anti-CREB	BF8028	1,2000	Affinity Biosciences, China
rabbit anti-eIF2	AF6087	1:1000	Affinity Biosciences, China
rabbit anti-MAP1A	ab184350	1:1000	abcam, UK
rabbit anti-MAP1B	DF12422	1:1000	Affinity Biosciences, China
rabbit anti-MAP2	Ab96378	1: 5000	abcam, UK
rabbit anti-MAP4	AF0079	1:1000	Affinity Biosciences, China
Mouse anti-Tau	66499-1-IG	1:1000	Proteintech Group, USA
rabbit anti-Actin	AF7018	1:1000	Affinity Biosciences, China

measured. Fifty micrograms of protein was loaded and separated by 10% SDS-PAGE and then transferred to PVDF membranes using a semi-dry electrotransfer system. The antibodies used in the Western blot analysis are listed in Table 3. The PVDF membranes were then washed and incubated with the corresponding secondary antibodies (1:10,000 dilution, Goat Anti-Mouse IgG, Goat Anti-Rabbit IgG, Bioswamp, China). The immunoblotting signals were detected by ECL (enhanced chemiluminescence) on chemiluminescence films. Blots were scanned and quantified using Band Scan software (Glycol

Biomedical, Canada), and GAPDH protein was expressed as a ratio of the target gene to detect immunoreactivity.

Statistical analysis

The data collected in the present study are expressed as mean \pm standard deviation (mean \pm SD) and were analyzed by one-way repeated measures ANOVA to determine differences between the two groups. Statistical analyses were performed using the statistical software program SPSS 26 (SPSS Inc, Chicago, USA). $P < 0.05$ was considered statistically significant.

Results

The effect of EA on MRI grade scores and ADC and FA values

In this study, we used T2, DWI and DTI mappings. We first evaluated whether the charger successfully induced the degeneration model on T2-weighted images. The results showed that the signal intensity of the intervertebral disc nucleus pulposus gradually decreased after axial compression, and the difference in signal intensity between healthy intervertebral discs and compressed discs was significant. This result is consistent with the findings of previous studies [23]. After EA intervention, a slight recovery of signal intensity was observed (Figure 2 A). Statistical analysis revealed that the Pfirrmann grading of the sham group was level 1 (Fig. 2C) and the mean values of ADC and FA were the highest. After pressurizing the intervertebral disc, the Pfirrmann grading can be elevated, and the ADC and FA values can be significantly reduced. Compared to the model group, the Pfirrmann grading decreased and the ADC and FA values increased after 28 days of EA intervention.

The effect of EA on AQP1 and AQP3 protein expression in IVDD

AQPs play an important role in maintaining cellular water homeostasis. In this study, AQP1 and AQP3 were found to be widely distributed in healthy discs using immunofluorescence detection (Fig. 3A). Compared with the sham groups, the immunofluorescence activity levels of AQP1 and AQP3 were significantly reduced in the compressed disc. However, the immunofluorescence expression of AQP1 and AQP3 increased in the degenerated disc after the electroacupuncture procedure (Fig. 3B, C). In addition, Western blot analysis and qRT-PCR were used to confirm the results.

Effect of EA on degenerative disc pathology

In the sham group, collagen displayed a uniform network structure within the nucleus pulposus matrix. The nucleus pulposus cells were evenly distributed in either single or clumpy aggregates. There was a substantial number of cells, which were round, oval, or spindle-shaped,

featuring large cell bodies and numerous inclusion bodies in the cytoplasm. The cartilage structure was distinct, and abundant chondrocytes were present, with large and round nuclei. Upon pressure treatment, the collagen arrangement within the nucleus pulposus matrix became disorganized, and collagen fiber deposition was irregular. Various-sized vacuoles emerged, aggregating into a fluffy mass, and cracks formed between cells, leading to necrosis of the nucleus pulposus tissue. The distribution of nucleus pulposus cells was uneven, and their number decreased significantly. Meanwhile, the remaining nodular cell inclusion bodies either significantly diminished or disappeared. After the EA procedure, the collagen distribution in the nucleus pulposus was largely uniform, and fiber deposition was strengthened. The nucleus pulposus cells enlarged in size, the inclusion bodies disappeared, and the cell gaps narrowed. The cartilage structure was clear, and the cartilage layer thickened (Figure 4 A).

Effect of EA on the levels of molecules related to the cAMP/PKA signaling pathway in IVDD

In the present study, we investigated whether the cAMP/PKA signaling pathway is also involved in the regulation of IVDD by EA. First, we used an ELISA assay to detect the expression levels of cAMP and PKA. The results showed that cAMP and PKA levels were significantly reduced in the model group compared to the sham group. EA significantly restored cAMP and PKA levels. (Figure 4B and C). Finally, Western blot and qRT-PCR analysis were used to examine the effect of EA on the molecular levels related to the cAMP/PKA signaling pathway in intervertebral disc degeneration. The results showed that the mRNA and protein levels of CREB, eIF-2, actin, MAP1A, MAP1B, MAP2, MAP4 and Tau were significantly decreased in the model group compared with the sham group. EA significantly restored the mRNA protein levels of CREB, eIF-2, actin, MAP1A, MAP1B, MAP2, MAP4 and Tau (Fig. 5A-Q).

Inhibition of PKA reverses the protective effect of EA on IVDD

Based on the above evidence, we further aimed to clarify the functions of cAMP/PKA signaling in EA protection of degenerative intervertebral discs. Initially, after successful modeling, we gave electroacupuncture intervention when the PKA inhibitor H-89 was injected into the disc. The production of cAMP and PKA was significantly reduced after pretreatment with the inhibitors, as confirmed by ELISA (Fig. 6A, B). Using Western blot and qRT-PCR analysis, we discovered that PKA repression reversed the protective effect of EA on degenerative intervertebral discs (Fig. 6C-W).

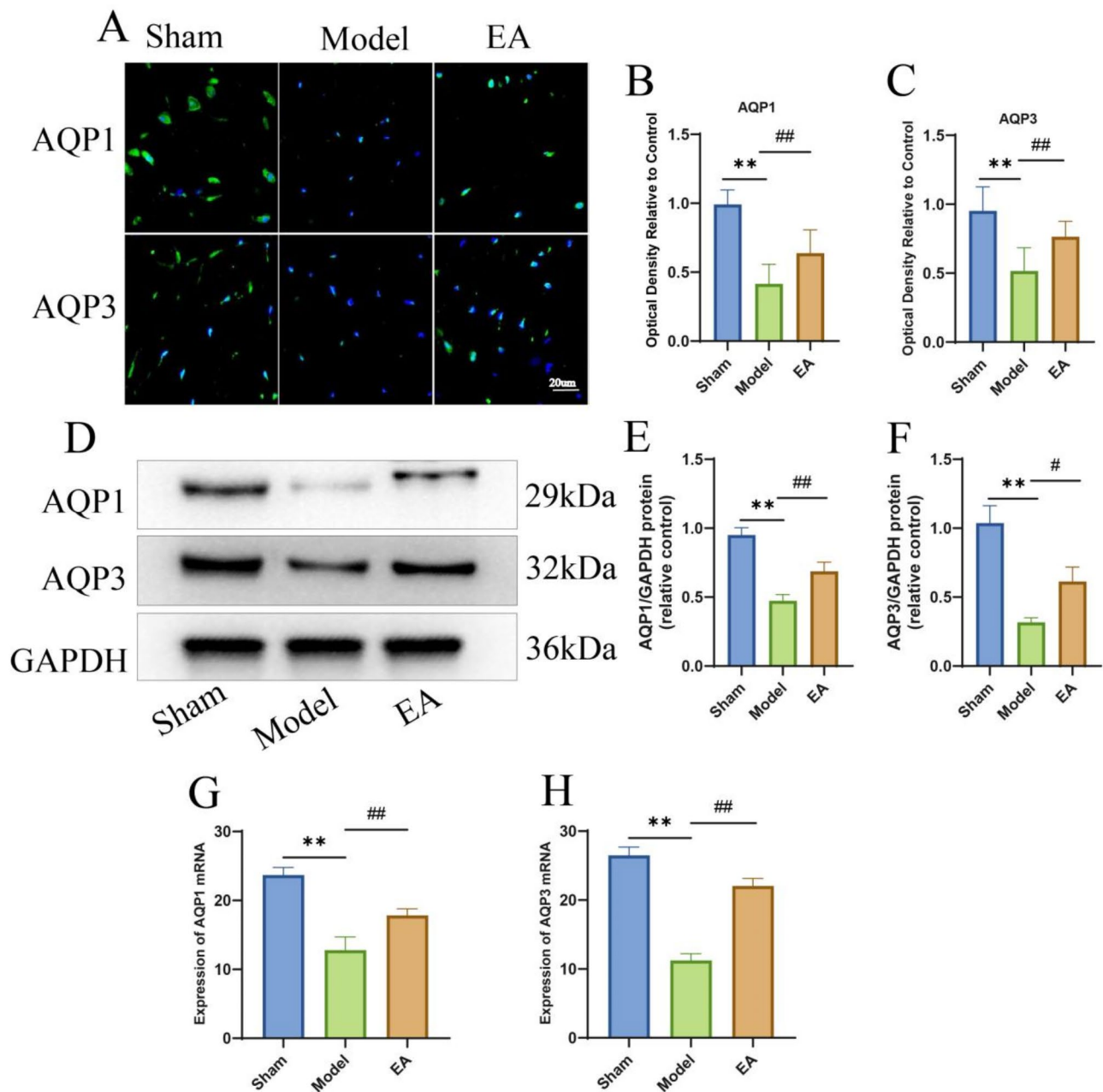


Fig. 3 AQP1 and AQP3 protein expression in disc degeneration. **(A)** Representative microscopic photographs of immunofluorescence staining showing AQP1 and AQP3 immunoreaction-positive products. Nuclei counterstained with DAPI showed blue, with AQP1 and AQP3 positive products appearing green. Scale bar: 20 μ m. The average optical density (AOD) was measured. **(B,C)** Bar graphs showing the AQP1 and AQP3 immunoreaction-positive products. **(D)** Western blot analysis of AQP1 and AQP3 protein levels. GAPDH was analyzed as a housekeeping gene. **(E, F)** Bar graphs showing the protein levels of AQP1 and AQP3. **(G, H)** Bar graphs showing the mRNA levels of AQP1 and AQP3. Data are expressed as mean \pm SD; ** P < 0.01 compared to the sham compressed group; ## P < 0.01 and # P < 0.05 compared to the model group

Discussion

The goal of this study was to detect whether EA can upregulate APQ expression in IVDD by regulating the cAMP/PKA pathway in a rabbit model of disc degeneration. Firstly, our findings demonstrate that dynamic loading causes a decrease in AQP expression and blocks water transport, thus resulting in biomechanical and structural

changes in disc cells. These changes were reversed after 28 days of EA treatment, suggesting that the EA stimuli promote cells to spontaneously recover from mechanical loading in vivo. Secondly, we found that EA significantly attenuated the decreased AQPs content and water diffusion, which were reversed by the cAMP/PKA pathway inhibitor H-89. Moreover, the expression levels of AQP1,

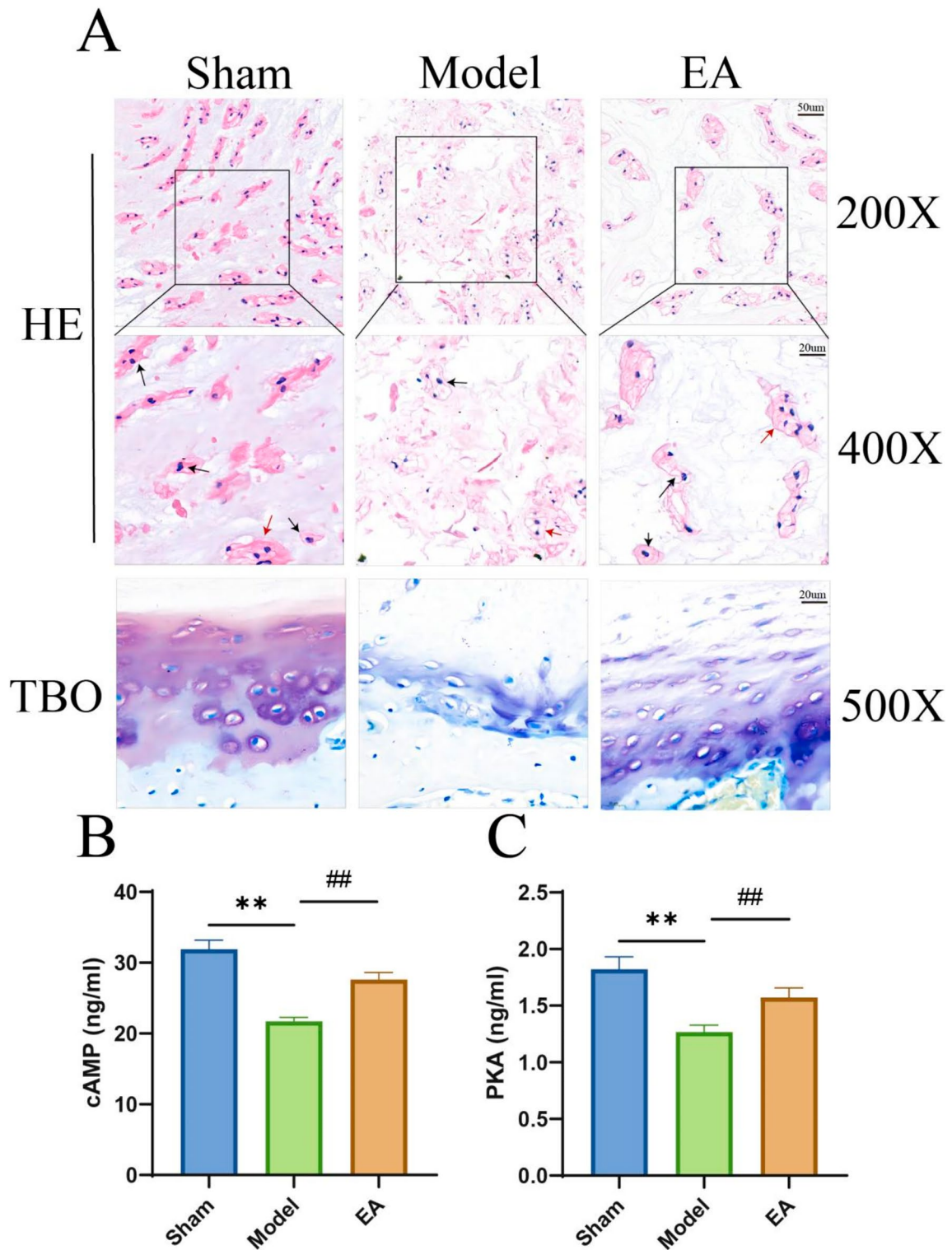


Fig. 4 Pathological morphology of the intervertebral disc and concentration expression of cAMP and PKA. **(A)** HE staining of nucleus pulposus cells. Scale bar: 20 μ m, 40 μ m; Toluidine blue staining of cartilage endplate cells. Toluidine blue stain can stain cartilage either purple or light blue. Scale bar: 50 μ m. **(B)** The cAMP level in the intervertebral disc. **(C)** The level of PKA in the intervertebral disc. Data are expressed as mean \pm SD; Asterisks indicate statistical significance (** P < 0.01 compared to the sham compressed group, ## P < 0.01 compared to the model group)

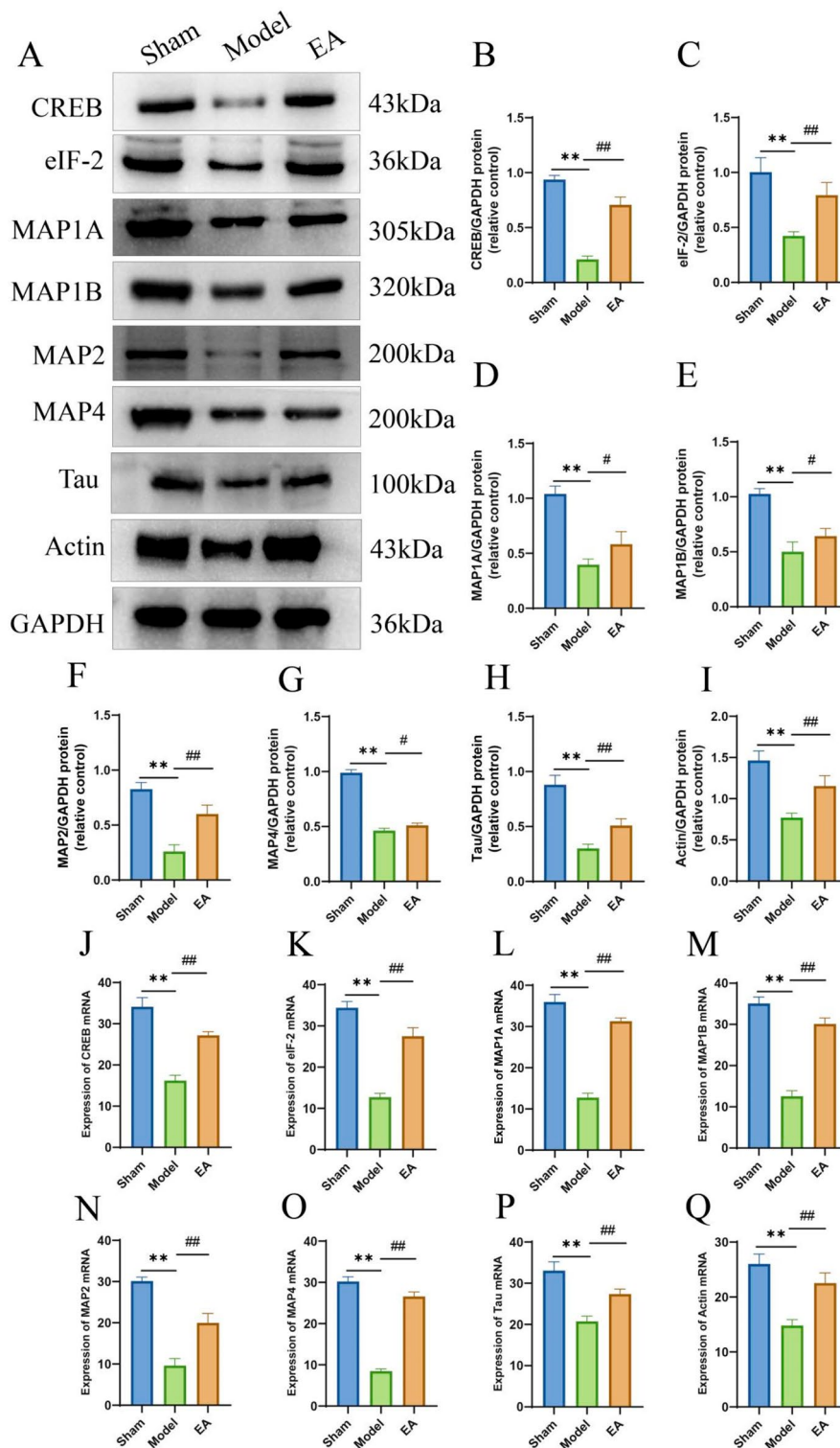


Fig. 5 Protein and mRNA levels of the cAMP/PKA pathway related molecules. **(A)** The protein levels of CREB, eIF-2, actin, MAP1A, MAP1B, MAP2, MAP4, and Tau in the lumbar disc. **(B-I)** Quantitative graphs representing the relative protein levels. **(J-Q)** The mRNA levels of CREB, eIF-2, actin, MAP1A, MAP1B, MAP2, MAP4, and Tau in the lumbar disc. Data are expressed as the mean \pm SD. ** $P < 0.01$, compared with the sham group; ## $P < 0.01$, compared with the model group

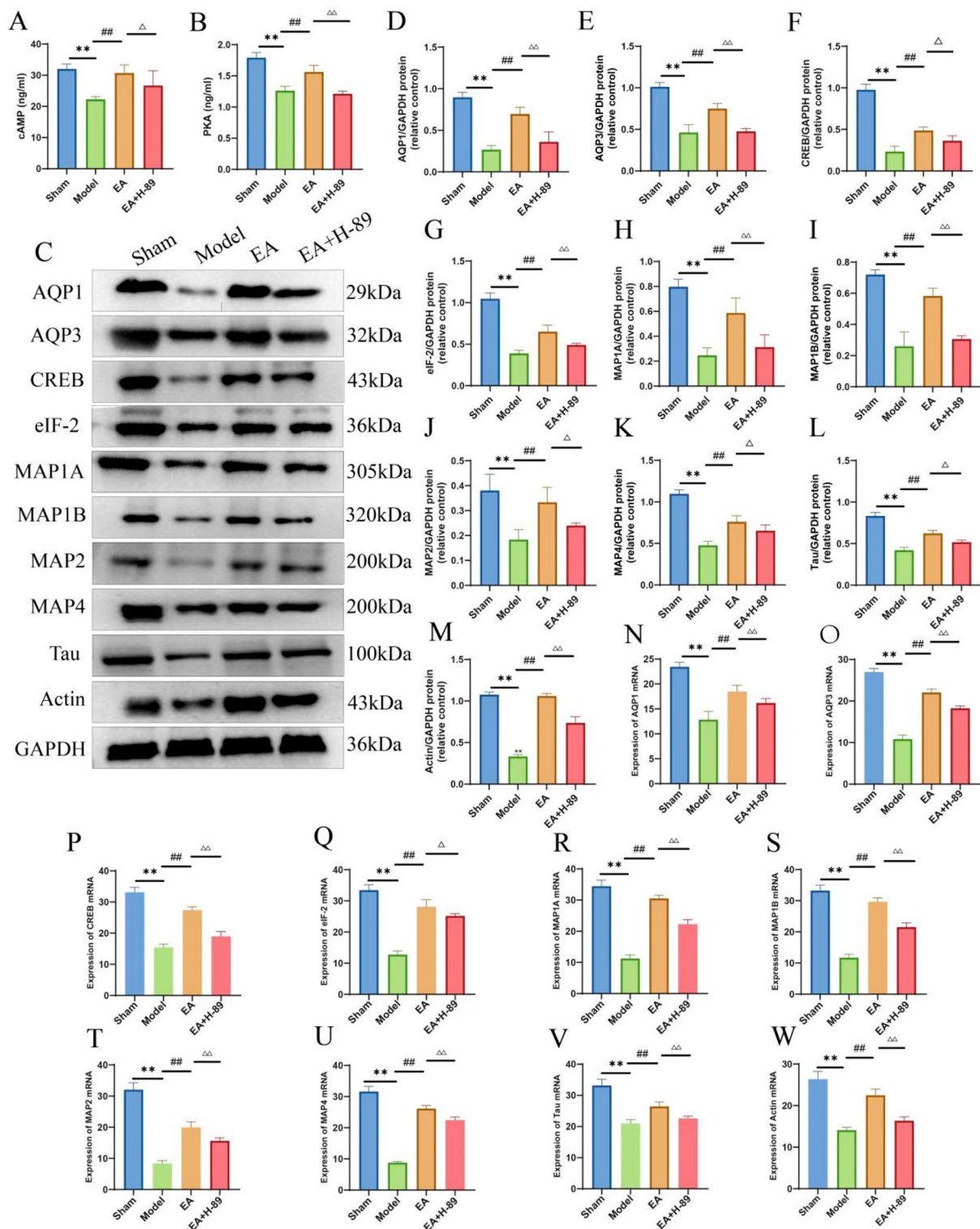


Fig. 6 Inhibition of PKA reverses the protective effect of EA on degenerative intervertebral discs. **(A)**The level of cAMP in the lumbar disc. **(B)**The level of PKA in the lumbar disc. **(C)**The protein levels of AQP1, AQP3, CREB, eIF-2, actin, MAP1A, MAP1B, MAP2, MAP4, and Tau in the lumbar disc. **(D-M)**The quantitative graphs of AQP1, AQP3, CREB, eIF-2, actin, MAP1A, MAP1B, MAP2, MAP4, and Tau. **(N-W)**The mRNA levels of AQP1, AQP3, CREB, eIF-2, actin, MAP1A, MAP1B, MAP2, MAP4, and Tau in the lumbar disc. Data are expressed as the mean \pm SD. ** $P < 0.01$, compared with the sham group; ## $P < 0.01$, compared with the model group; $\Delta\Delta P < 0.01$, $\Delta P < 0.05$, compared with the EA group

AQP3 and the cAMP/PKA pathway were reduced in IDD rabbits compared with the sham group rabbits. EA significantly restored the expression of AQP1, AQP3, and the cAMP/PKA pathway, while H-89 significantly reversed the effects of EA on protein and mRNA expression.

The intervertebral disc (IVD) is a highly hydrated tissue consisting of the nucleus pulposus, annulus fibrosus, and cartilaginous endplate. The central NP is a site of collagen secretion and contains numerous proteoglycans, which facilitate water retention, creating hydrostatic pressure to resist axial compression of the spine [35, 36]. It is well acknowledged that mechanical stress is one of the key contributors to intervertebral disc degeneration [37]. Disc degeneration is characterized by changes in ECM properties, including loss of proteoglycans and collagens, degenerative fibrillation, and decreased water content [38, 39], which alter the disc's ability to bear load. As degenerated intervertebral discs contain less water and therefore inferior capabilities for sustaining pressure, they bulge and lose height. We first established a disc degeneration animal model using a homemade loading device *in vivo*. The observed biological mechanisms are consistent with human characteristics [40, 41]. This similarity conveys the primary advantage of longitudinal investigation.

In this study, the MRI method was used to evaluate whether the model was successfully established first. Sagittal T2 images showed a significant decrease in nucleus pulposus hydration after 28 days of compression, in contrast to the control or sham group. Based on sagittal T2-weighted images of the nucleus pulposus signal changes. The intervertebral disc was divided into five levels according to the Pfirrmann IVDD grading standards [42]. The results showed that grade IV or V degenerative changes were detected at 28 days after compression, and the sham group was grade I on T2-weighted imaging. One of the latest advancements in MRI technology is the application of DWI and DTI. This reflects the microstructural changes in tissue by describing the diffusion of water molecules. DWI is used to detect the capacity of water diffusion and generates ADC images; DTI describes the directional characteristics of water diffusion and produces FA images. In the present study, the mean ADC and FA values of different groups closely coincided with the biochemical characteristics. Higher contents of PG and water in the control and sham groups appeared to correspond with higher ADC values and FA values. The disc in the compression group showed decreased ADC and FA values, suggesting that the water content gradually declined and that ECM degradation in the loading status intervention effectively increased both the ADC and FA values. EA showed a significant therapeutic effects and regeneration potential in IVDD by improving water molecule transportation.

It is acknowledged that water enters cells through diffusion, permeation, and specialized transportation channels. As water is transported, nutrition and metabolism products are also transported. Water transmembrane transportation is important for maintaining normal metabolism in cells. AQPs are a thirteen-member family of water channels, driven by osmotic gradients [43]. Since AQPs' expression was observed to be sensitive to disc degeneration [18], it was of interest to study their expression and regulation in disc tissues. There is indirect evidence suggesting that AQPs are crucial in maintaining cellular water homeostasis under dynamic osmotic conditions and have been shown to cotransport many important metabolites such as CO₂ and O₂ [44, 45]. Aquaporin 1 is a transport channel for water and is widely expressed in systemic cells. Aquaporin 3 can also transport glycerol. Previous studies have suggested the importance of water transport across the cell membrane in resident chondrocyte-like cells for volume regulation in response to mechanical stimuli and changes in osmolarity [46]. Previous studies have shown that AQP1 is associated with greater disc hydration [14], and AQP3 can protect against lumbar IDD via the Wnt/ β -catenin pathway [47]. Our results clearly show that the levels of both AQP1 and AQP3 are lower in discs with progressive degeneration. Western blot analysis and immunofluorescence microscopy, respectively, indicated that AQP protein expression was decreased in loading-induced discs compared to that in non-degenerative discs. 28 days of EA treatment upregulated the AQP protein expression, and the AQP content was obviously lower in the EA group than in the untreated group. These results provide further support for observations by Wang et al. [48], who showed differential expression of AQP in young versus aged rabbit discs, suggesting a possible role for AQPs in age-related degeneration of the disc in terms of the ability of the matrix to bind water, thus maintaining the biomechanical function of the intervertebral disc.

cAMP is an important substance for tissue cells to maintain physiological functions, and PKA is one of its main target proteins. cAMP can bind to the regulatory subunit of PKA, thus promoting the phosphorylation of PKA and forming a complete cAMP/PKA activation pathway [49]. G proteins induce and activate adenylate cyclase, which increases the content of cAMP and induces the activation of PKA, thereby regulating the expression level of AQPs and increasing water reabsorption [50]. The cAMP-PKA pathway is involved in the mechanism of irritable bowel syndrome by the regulation of AQPs [51]. Recently, the cAMP/PKA pathway has been reported to participate in the treatment of EA in rats with depression and pain memory [52, 53]. These reports indicate that the cAMP/PKA pathway may play a role in the treatment of EA in diseases. In our study, we found that

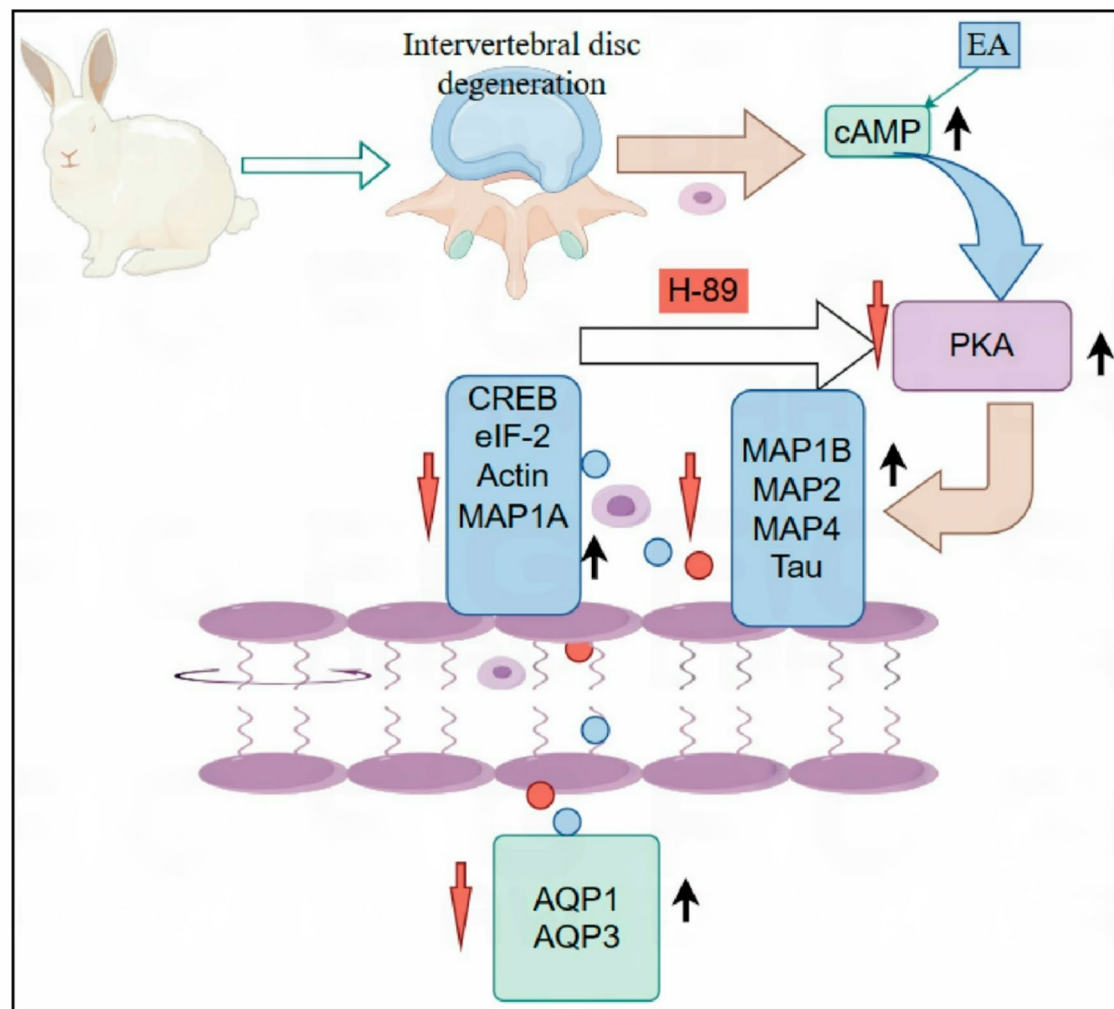


Fig. 7 Protective mechanism of EA on IVDD. EA may delay IVDD by activating the cAMP/PKA signaling pathway to promote intervertebral disc material transport. The black arrow shows the effect of electroacupuncture, and the red arrow shows the reversing effect of H-89 on the electroacupuncture

the level of the cAMP/PKA pathway was significantly decreased in disc degeneration rabbits as compared with sham group rabbits. EA treatment significantly restored the decreased level of the cAMP/PKA pathway, which was then reversed by H-89, indicating that EA may play a therapeutic role through its action on the cAMP/PKA pathway. We further examined the expression levels of AQP1 and AQP3, as well as key molecules in the cAMP/PKA pathway, and found that EA significantly restored the mRNA and protein levels of AQP1, AQP3, CREB, eIF-2, actin, MAP1A, MAP1B, MAP2, MAP4, and Tau, while the mRNA and protein levels of these molecules were reversed by H-89. These results further demonstrate that EA may attenuate disc degeneration through regulation of the expression of AQP1 and AQP3 via the cAMP/PKA pathway.

Conclusions

In summary, the author performed this study to determine the effect of EA treatment on AQP expression in degenerated discs. We found that mechanical loading induces disc degeneration and that AQP1 and AQP3 are closely correlated with the progression of IVDD. EA expedited the transportation of nutrition and metabolism substances by increasing the hydration degree and permeability of the disc cells. This finding suggests that EA therapy may restore the biophysical properties of disc cells and that EA may play a protective role by targeting AQP1 and AQP3 via the cAMP/PKA pathway. Additionally, our findings provide an experimental and theoretical basis for the clinical treatment of low back pain (Fig. 7).

Acknowledgements

We thank the members of the research team at the College of Acupuncture and Bone Injury, Hubei University of Traditional Chinese Medicine, Yan Lin Zhang, Kun Xiu Wang, Chen Pei, et al. We would like to thank the Animal

Research Center for all the help they have given us in raising our laboratory animals.

Author contributions

WM and HJB performed the Western blot, immunostaining and EA treatment. HJB and ZJ analyzed the data. HGF designed and supervised the study. WM and ZJ wrote the manuscript. All authors reviewed the manuscript.

Funding

This work was supported financially by the National Natural Science Foundation of China General Program (Nos. 81574072, 81774392, 82074517, and 82374592).

Data availability

No datasets were generated or analysed during the current study.

Declarations

Ethics approval and consent to participate

All procedures were approved by the Animal Care Committee at Wuhan Hospital of Integrated Chinese & Western Medicine.

Competing interests

The authors declare no competing interests.

Received: 9 September 2024 / Accepted: 17 March 2025

Published online: 25 March 2025

References

- Global burden. Of 369 diseases and injuries in 204 countries and territories, 1990–2019: a systematic analysis for the global burden of disease study 2019[J]. *Lancet*. 2020;396(10258):1204–22.
- CIEZA A, CAUSEY K, KAMENOV K, et al. Global estimates of the need for rehabilitation based on the global burden of disease study 2019: a systematic analysis for the global burden of disease study 2019[J]. *Lancet*. 2021;396(10267):2006–17.
- LIU C, LIU L, YANG M, et al. A positive feedback loop between EZH2 and NOX4 regulates nucleus pulposus cell senescence in age-related intervertebral disc degeneration[J]. *Cell Div*. 2020;15:2.
- XING H, ZHANG Z, MAO Q, et al. Injectable exosome-functionalized extracellular matrix hydrogel for metabolism balance and pyroptosis regulation in intervertebral disc degeneration[J]. *J Nanobiotechnol*. 2021;19(1):264.
- TIAN D, LIU J, CHEN L, et al. The protective effects of PI3K/Akt pathway on human nucleus pulposus mesenchymal stem cells against hypoxia and nutrition deficiency[J]. *J Orthop Surg Res*. 2020;15(1):29.
- KANNA R M RAJASEKARAN S. How reliable are the reported genetic associations in disc degeneration?? The influence of phenotypes, age, population size, and inclusion sequence in 809 Patients[J]. *Spine (Phila Pa 1976)*. 2016;41(21):1649–60.
- KIRNAZ S, CAPADONA C, WONG T, et al. Fundamentals of intervertebral disc Degeneration[J]. *World Neurosurg*. 2022;157:264–73.
- HE R, WANG Z, CUI M, et al. HIF1A alleviates compression-induced apoptosis of nucleus pulposus derived stem cells via upregulating autophagy[J]. *Autophagy*. 2021;17(11):3338–60.
- YIN X, MOTORWALA A, VESVORANAN O, et al. Effects of glucose deprivation on ATP and proteoglycan production of intervertebral disc cells under Hypoxia[J]. *Sci Rep*. 2020;10(1):8899.
- SADOWSKA A, KAMEDA T, KRUPKOVA O, et al. Osmosensing, osmosignaling and inflammation: how intervertebral disc cells respond to altered osmolarity[J]. *Eur Cell Mater*. 2018;36:231–50.
- YANG B, O'CONNELL G. D. Intervertebral disc swelling maintains strain homeostasis throughout the annulus fibrosus: A finite element analysis of healthy and degenerated discs[J]. *Acta Biomater*. 2019;100:61–74.
- GALBUSERA F, van RIJSBERGEN M, ITO K, et al. Ageing and degenerative changes of the intervertebral disc and their impact on spinal flexibility[J]. *Eur Spine J*. 2014;23(Suppl 3):S324–32.
- COLOMBIER P, CLOUET J, HAMEL O, et al. The lumbar intervertebral disc: from embryonic development to degeneration[J]. *Joint Bone Spine*. 2014;81(2):125–9.
- HOFFMAN H, CHOI A W CHANGV, et al. Aquaporin-1 expression in herniated human lumbar intervertebral Discs[J]. *Global Spine J*. 2017;7(2):133–40.
- LI SB, YANG K S, ZHANG, Y T. Expression of Aquaporins 1 and 3 in degenerative tissue of the lumbar intervertebral disc[J]. *Genet Mol Res*. 2014;13(4):8225–33.
- De GEERCM. Intervertebral disk nutrients and transport mechanisms in relation to disk degeneration: A narrative literature Review[J]. *J Chiropr Med*. 2018;17(2):97–105.
- XU Y, YAO H, WANG Q, et al. Aquaporin-3 attenuates oxidative Stress-Induced nucleus pulposus cell apoptosis through regulating the P38 MAPK Pathway[J]. *Cell Physiol Biochem*. 2018;50(5):1687–97.
- SNUGGS JW, DAY R E, BACH F C, et al. Aquaporin expression in the human and canine intervertebral disc during maturation and degeneration[J]. *JOR Spine*. 2019;2(1):e1049.
- MENGRUI Z, CHAO L. Efficacy of bloodletting combined with Tongji electroacupuncture on patients with lumbar disc herniation sciatica and its influence on functional recovery and pain status[J]. *Shaanxi J Traditional Chin Med*. 2023;44(08):1141–4.
- TIAN M, YANG Y, QIN W, et al. Electroacupuncture promotes nerve regeneration and functional recovery through regulating LncRNA GAS5 targeting miR-21 after sciatic nerve injury[J]. *Mol Neurobiol*. 2024;61(2):935–49.
- MU J, FURLAN A D, LAM W Y, et al. Acupuncture for chronic nonspecific low back pain[J]. *Cochrane Database Syst Rev*. 2020;12(12):CD13814.
- EZEMA C I, ONYESO O K, NNA E O, et al. Transcutaneous electrical nerve stimulation effects on pain-intensity and endogenous opioids levels among chronic low-back pain patients: A randomised controlled trial[J]. *J Back Musculoskelet Rehabil*. 2022;35(5):1053–64.
- CHEN W, CHEN Y, CHENG W, et al. Acupuncture exerts preventive effects in rats of chronic unpredictable mild stress: the involvement of inflammation in amygdala and brain-spleen axis[J]. *Biochem Biophys Res Commun*. 2023;646:86–95.
- DUAN DM, DONG X, TU Y, et al. A microarray study of chronic unpredictable mild stress rat blood serum with electro-acupuncture intervention[J]. *Neurosci Lett*. 2016;627:160–7.
- WU Q, CHEN J, YUE J, et al. Electroacupuncture improves neuronal plasticity through the A2AR/cAMP/PKA signaling pathway in SNL rats[J]. *Neurochem Int*. 2021;145:104983.
- CASSIDY JD, YONG-HING K, KIRKALDY-WILLIS W H, et al. A study of the effects of bipedism and upright posture on the lumbosacral spine and paravertebral muscles of the Wistar rat[J]. *Spine (Phila Pa 1976)*. 1988;13(3):301–8.
- GLOOBE H. Osteophyte formation in experimental bipedal rats[J]. *J Comp Pathol*. 1973;83(1):133–41.
- KROEBER M, UNGLAUB F, GUEHRING T, et al. Effects of controlled dynamic disc distraction on degenerated intervertebral discs: an in vivo study on the rabbit lumbar spine model[J]. *Spine*. 2005;30(2):181–7.
- KROEBER M W, UNGLAUB F, WANG H, et al. New in vivo animal model to create intervertebral disc degeneration and to investigate the effects of therapeutic strategies to stimulate disc regeneration[J]. *Spine (Phila Pa 1976)*. 2002;27(23):2684–90.
- HUANG G, ZOU J, SHI J, et al. The effect of electroacupuncture on the extracellular matrix synthesis and degradation in a rabbit model of disc degeneration.[J]. *Evidence-based Complement Altern Medicine: eCAM*. 2014;2014:731395.
- ZHANG Y, ZOU J, WANG M, et al. Effect of electroacupuncture at Jiaji (EX-B2) on senescence of nucleus pulposus cells of degenerated lumbar intervertebral disc in rabbits.[J]. *Zhen Ci Yan jiu = Acupunct Res*. 2023;48(10):1001–8.
- ZHANG ZHANGMLIANGC. Effects of electroacupuncture at Jiaji points on inflammation, nucleus pulposus cell cycle and FADD/Caspase-8 signaling pathway in rat degenerated lumbar Disc[J]. *J Guangzhou Univ Chin Med*. 2024;41(11):2985–91.
- ZOU J, JIANG M, LI J, et al. Effect of electroacupuncture at Jiaji points (EX-B2) on nucleus proteoglycan expression in rabbits model with lumbar disc Degeneration[J]. *Chin J Integr Med*. 2018;38(02):223–6.
- LIU F, XU Y, WANG Y, et al. Real-time PCR analysis of PAMP-induced marker gene expression in *Nicotiana benthamiana*[J]. *Bio Protoc*. 2018;8(19):e3031.
- KADOW T, SOWA G, VO N, et al. Molecular basis of intervertebral disc degeneration and herniations: what are the important translational questions?[J]. *Clin Orthop Relat Res*. 2015;473(6):1903–12.
- GOPAL D, HO A L, SHAH A, et al. Molecular basis of intervertebral disc degeneration[J]. *Adv Exp Med Biol*. 2012;760:114–33.

37. FU F, BAO R. Aberrant spinal mechanical loading stress triggers intervertebral disc degeneration by inducing pyroptosis and nerve ingrowth[J]. *Sci Rep.* 2021;11(1):772.
38. LIANG H, LUO R, LI G et al. The proteolysis of ECM in intervertebral disc Degeneration[J]. *Int J Mol Sci.* 2022;23(3).
39. ZHANG S, LIU W, CHEN S, et al. Extracellular matrix in intervertebral disc: basic and translational implications[J]. *Cell Tissue Res.* 2022;390(1):1–22.
40. LOTZ JC, COLLIUO O K CHINJR, et al. Compression-induced degeneration of the intervertebral disc: an in vivo mouse model and finite-element study[J]. *Spine.* 1998;23(23):2493–506.
41. SHI S, KANG X, ZHOU Z, et al. Excessive mechanical stress-induced intervertebral disc degeneration is related to Piezo1 overexpression triggering the imbalance of autophagy/apoptosis in human nucleus pulpous.[J]. Volume 24. *Arthritis research & therapy.* 2022. p. 119. 1.
42. PFIRRMANN C W, METZDORF A, ZANETTI M, et al. Magnetic resonance classification of lumbar intervertebral disc degeneration[J]. *Spine (Phila Pa 1976).* 2001;26(17):1873–8.
43. DAY RE, KITCHEN P, OWEN D S, et al. Human Aquaporins: regulators of transcellular water flow[J]. *Biochim Biophys Acta.* 2014;1840(5):1492–506.
44. ZWIAZEK JJ, XU H, TAN X, et al. Significance of oxygen transport through aquaporins[J]. *Sci Rep.* 2017;7:40411.
45. GROSZMANN M, OSBORN H L, EVANS JR. Carbon dioxide and water transport through plant aquaporins[J]. *Plant Cell Environ.* 2017;40(6):938–61.
46. SNUGGS JW, TESSIER S, BUNNING R, et al. TonEBP regulates the hyperosmotic expression of Aquaporin 1 and 5 in the intervertebral disc[J]. *Sci Rep.* 2021;11(1):3164.
47. XIE H, JING Y, XIA J, et al. Aquaporin 3 protects against lumbar intervertebral disc degeneration via the Wnt/beta-catenin pathway[J]. *Int J Mol Med.* 2016;37(3):859–64.
48. WANG Q, LI Y, WU C, et al. Aquaporin-1 Inhibition exacerbates ischemia-reperfusion-induced lung injury in mouse[J]. *Am J Med Sci.* 2023;365(1):84–92.
49. VENKATAKRISHNAN V, GHODE A, TULSIAN N K, et al. Impaired cAMP processivity by phosphodiesterase-protein kinase A complexes in acrodysostosis[J]. *Front Mol Biosci.* 2023;10:1202268.
50. LIN L, JIANG Y, LIN P, et al. Classical famous prescription of Jichuan Decoction improved loperamide-induced slow transit constipation in rats through the cAMP/PKA/AQPs signaling pathway and maintained inflammatory/intestinal flora homeostasis[J]. *Heliyon.* 2024;10(1):e21870.
51. CHAO G, ZHANG S. Aquaporins 1, 3 and 8 expression and cytokines in irritable bowel syndrome rats' colon via cAMP-PKA pathway[J]. *Int J Clin Exp Pathol.* 2018;11(8):4117–23.
52. LIU JH, WU Z F, SUN J, et al. Role of AC-cAMP-PKA cascade in antidepressant action of electroacupuncture treatment in Rats[J]. *Evid Based Complement Alternat Med.* 2012;2012:932414.
53. SUN J, FANG J Q, SHEN Z, et al. [Comparison of the effect between electroacupuncture and NSAIDs on pain memory based on cAMP/PKA/CREB pathway in anterior cingulate gyrus][J]. *Zhongguo Zhen Jiu.* 2020;40(4):397–404.

Publisher's note

Springer Nature remains neutral with regard to jurisdictional claims in published maps and institutional affiliations.